Quantitative assessment and thermodynamic modelling of microstructural stability in a new nitrogen-rich super duplex weld metal

A. Gregori, J.-O. Nilsson

Multipass gas tungsten arc welding with a shielding gas of Ar+2%N_2 was used to produce superduplex weld metals employing an established filler metal of the type 25%Cr-10%Ni-4%Mo-0.28%N and the new filler metal of type 29%Cr-8%Ni-2%Mo-0.4%N. Investigations in the temperature range 700-1050°C showed that intermetallic phase in type 25Cr10Ni4Mo was of two kinds, viz. σ–phase and χ–phase. However in type 29Cr8Ni2Mo weld metal only σ–phase was identified. The tendency to form secondary austenite in reheated weld beads was significantly reduced in type 29Cr8Ni2Mo weld metal, owing to the faster kinetics of austenite formation expected in high-nitrogen weld metal. The microstructure of type 29Cr8Ni2Mo weld metal was found to be more stable with respect to intermetallic phase formation than that of type 25Cr10Ni4Mo. This is in part explicable in terms of the effect of nitrogen on the driving force for the decomposition of ferrite into σ–phase and austenite. Calculations using the computer program Thermo-Calc showed that the driving force for σ–phase decreased with additions of nitrogen, which can be understood physically in terms of a lower activity of chromium and molybdenum in the presence of nitrogen.

INTRODUCTION

The demand for stainless steels with enhanced characteristics in terms of corrosion resistance and mechanical strength under severe environmental conditions has been the driving force for developing new high alloy duplex stainless steels (DSS). Duplex grades with increased contents of alloying elements are superior to most austenitic steels because of their resistance to localised corrosion. Unfortunately, it so happens that elements, such as chromium and molybdenum, that enhance pitting resistance lead to a higher susceptibility to precipitation of deleterious intermetallic phases [1, 2]. Introduction of high nitrogen levels in recently developed DSS looks extremely promising [3].

Phase transformations taking place during welding in both the heat affected zone (HAZ) and the weld metal, have a great influence on properties and microstructure. A crucial factor in making optimum use of DSS is to produce welded joints with properties matching those of the base metal. Optimum weldability requires that filler metals be developed in close relation to the base metal. Nitrogen-rich weld metal correlates with a more homogeneous microstructure and a lower volume fraction of secondary austenite formed from unstable ferrite after reheating but it also acts to reduce the difference in ferrite amount between as solidified and reheated parts of a multipass weld [4]. This reduction of secondary austenite, which has a low chromium and nitrogen content, contributes to improve the corrosion resistance [5]. Another effect of the nitrogen addition is the higher stability of the weld microstructure in terms of transformation of the ferrite into intermetallic phases [6]. In addition to its stabilising effects on the weld metal microstructure, nitrogen increases the pitting corrosion resistance. Consequently, nitrogen loss during welding or filler metal with low nitrogen may be detrimental for the critical pitting temperature [7].

The aim of the present investigation was to study the microstructural stability of a new high nitrogen DSS weld metal recently developed for the urea industry. Particular attention was paid to precipitation of intermetallic phases and secondary austenite.

EXPERIMENTAL

Two DSS weld metals were produced using the new filler metal of type 29.8.2 (denoted SDN) and a filler metal of the type 25.10.4.L adapted for SAF 2507 (here denoted SD). Multipass welding was employed using the GTAW technique with Ar + 2%N_2 shielding gas and a heat input of 1.2 kJ/mm. The resulting composition of the weld metal and the

A. Gregori,
University of Padova, Vicenza.

J. O. Nilsson,
Department of Physical Metallurgy, AB Sandvik Steel, Sweden.

Paper presented at the International Conference Stainless Steel'99, Chia Laguna, 6-9 June 1999, organised by AIM

Filler metal	Designation	C	Si	Mn	Cr	Ni	Mo	Cu	N	PRE (1)
25.10.4.L	SD	0,015	0,32	0,47	24,7	9,4	3,93	0,06	0,28	42
29.8.2	SDN	0,012	0,23	0,83	28,8	8,1	2,03	0,03	0,39	42

(1) PRE=Cr+3.3Mo+16N

Table 1. Chemical composition (wt. %) of the weld metals.

Tabella 1. Composizione chimica (% in peso) dei cordoni di saldatura investigati.

corresponding pitting resistance equivalent (PRE) are given in Table 1.

Isothermal heat treatments were performed in the temperature range 700-1050 °C for times ranging from 10 seconds to 72 hours, followed by water quenching. The volume fractions of δ, γ and intermetallic phases were measured by automatic image analysis (Kontron KS300 system) coupled to a Reichert MEF4 M light optical microscope. The contrast among different phases was enhanced using a modified Beraha etchant (0.7 g $K_2S_2O_5$, 20 ml HCl and 80 ml H_2O). The δ and σ amounts were also estimated by manual point counting (ISO 9042) and compared with the values obtained by automatic image analysis. The magnetic balance provided an independent method of measuring δ volume fraction (Table 2).

The calculation of the TTT and CCT diagrams, based on the experimental results obtained by image analysis, was performed assuming that the isothermal precipitation of intermetallic phases could be described by an Avrami equation [8-10]. The calculation of CCT diagrams was based on the assumption that the additivity rule proposed by Scheil [11] can be applied to the transformations occurring in DSS. In the present investigation a program developed by the authors [12, 13] was used to perform the calculation.

Microstructural investigations were carried out using a JEOL JSEM 840 scanning electron microscope (SEM) provided with a LINK ISIS unit for EDX analysis as well as an analytical transmission electron microscope (ATEM) of type JEOL 2000FX to identify precipitates by means of selected area (SAED) and convergent beam (CBED) electron diffraction. All diffraction work was performed using a double tilt specimen holder.

MICROSTRUCTURE

Weld metals consisted of primary ferrite grains with austenite mainly in the form of Widmanstätten precipitates. Areas where the ferrite had a "vermicular" appearance were located mainly interdendritically and formed an almost continuous network. Furthermore, its volume fraction was significantly lower than in the Widmanstätten regions. The vermicular regions solidified in a ferritic-austenitic mode rather than fully ferritic as in the Widmanstätten areas [14]. The ferrite content in the as-welded condition was clearly higher in the 29Cr8Ni2Mo weld metal than in 25Cr10Ni4Mo (Figure 1). Tilting experiments performed in the ATEM showed that ferrite and austenite in the normal duplex microstructure obeyed the Kurdjumov-Sachs law whereas δ and γ in the vermicular regions had no well-defined orientation relationship. It was observed that the ⟨001⟩ direction in ferrite deviated by 10 -18° from the ⟨011⟩ direction in austenite. In the as-welded condition no intermetallic phases were detected in the weld metals. However, intergranular precipitation of Cr_2N was occasionally observed in type 29Cr8Ni2Mo weld metal. These were observed mainly at ferrite/austenite grain boundaries and showed disc-like or lenticular morphologies (Figure 2). Small intragranular secondary austenite grains were visible in ferrite. These precipitates were inhomogeneously distributed and mainly located in the Widmanstätten reheated zones between two runs. It was qualitatively observed that the volume fraction of γ_2 is higher in the SD than in SDN weld metal. This reduction of secondary austenite is clearly related to the higher nitrogen content that stabilises the microstructure. A large number of γ_2 grains had sharp edges even if globular γ_2 were present in all weld metals (Figure 3).

Intermetallic phase precipitation of mainly sigma phase occurred during heat treatment of the weld metals at both δ/δ grain boundaries and δ/γ phase boundaries. LOM investigation clearly showed that 29.8.2 weld metal was less sensitive to intermetallic phase formation than the 25.10.4 weld metal (Table 3). It was observed that the ferrite morphology influenced the precipitation kinetics. Investigation of all weld metal showed that the intermetallic phases precipitated preferentially in the region where ferrite had a vermicular appearance with narrow arms. This was particularly evident in 25.10.4 whereas distribution of sigma phase was found to be much more uniform in 29.8.2 weld metal.

Long-term isothermal heat treatments showed that only minute amounts of intermetallic phase was present in 29Cr8Ni2Mo weld metal after ageing at 1000°C while material aged at 1050°C was devoid of intermetallic phase indicating that the dissolution temperature is in the interval 1000-1050°C, i.e. about 50°C lower than that of type 25Cr10Ni4Mo weld metal.

The morphology of sigma phase after 72 h depends on the temperature. At higher temperatures large coherent σ parti-

	29Cr8Ni2Mo	25Cr10Ni4Mo
Image Analysis	47,1±1,6	33,3±1,6
Manual Point Count	43,2±4,7	29,0±2,9
Magnetic Balance	46,4	30,0

Table 2. Volume fraction of ferrite in the unaged condition obtained by image analysis, manual point counting and magnetic balance

Tabella 2. Frazione volumetrica di ferrite misurata tramite analisi d'immagine, conteggio manuale e bilancia magnetica, nel materiale non trattato.

*Table 3. Volume fraction of intermetallic phase in 29Cr8Ni2Mo (SDN) and 25Cr10Ni4Mo (SD) weld metals determined by image analysis (** intermetallic phase volume fraction lower than 0.1%).*

*Tabella 3. Frazione volumetrica di fase intermetallica misurata tramite analisi d'immagine nel cordone di tipo 29Cr8Ni2Mo (SDN) e 25Cr10Ni4Mo (SD) (** frazione volumetrica inferiore allo 0,1%).*

Material	Temperature	Time 30 s	90 s	270 s	810 s	2430 s	7290 s	72 h
SDN	1050°C		0,00	0,00	0,00	0,00	0,00	0,00
SD			0,1±0,1	**	**	6,4±0,5	7,0±0,9	7,3±0,8
SDN	1000°C	0,00	0,00	0,00	0,00	0,1±0,1	0,1±0,1	0,7±0,2
SD		0,2±0,1	2,0±0,5	3,5±0,9	5,1±1,0	13,7±0,9	21,9±1,0	27,0±1,4
SDN	950°C	0,00	0,00	**	**			19,9±1,1
SD		0,3±0,1	1,4±0,3	4,1±0,6	7,1±0,5			30,4±1,2
SDN	900°C	0,00	**	0,2±0,1	0,9±0,2			20,0±0,8
SD		0,2±0,1	2,8±0,6	-	10,7±1,0			23,9±0,8
SDN	850°C	0,00	**	0,6±0,2	3,2±0,3			28,6±1,4
SD		**	0,5±0,2	2,5±0,5	7,2±0,7			24,3±0,9
SDN	800°C	0,00	0,00	**	0,7±0,2	2,2±0,4		16,9±1,8
SD		**	0,00	0,4±0,1	1,6±0,2	3,0±0,3		19,0±1,0
SDN	750°C			0,00	0,00	1,3±0,3	3,7±0,7	11,7±0,8
SD				**	0,3±0,1	0,9±0,2	2,4±0,2	16,5±1,1
SDN	700°C				0,00	0,00	0,1±0,1	5,5±0,9
SD					**	0,1±0,1	0,6±0,1	5,1±0,4

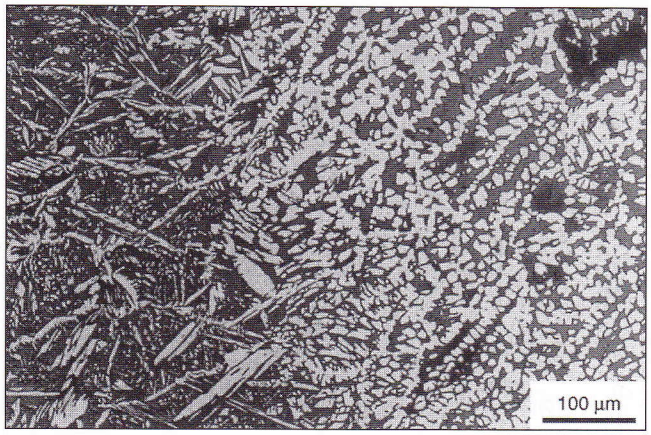

Figure 1. Microstructure of 29Cr8Ni2Mo weld metal consisting of regions with a Widmanstätten (left) and vermicular (right) morphology (γ bright phase).

Figura 1. Microstruttura del cordone di saldatura 29Cr8Ni2Mo costituito da regioni a morfologia Widmanstätten (sinistra) e vermicolare (destra) (γ è la fase chiara)

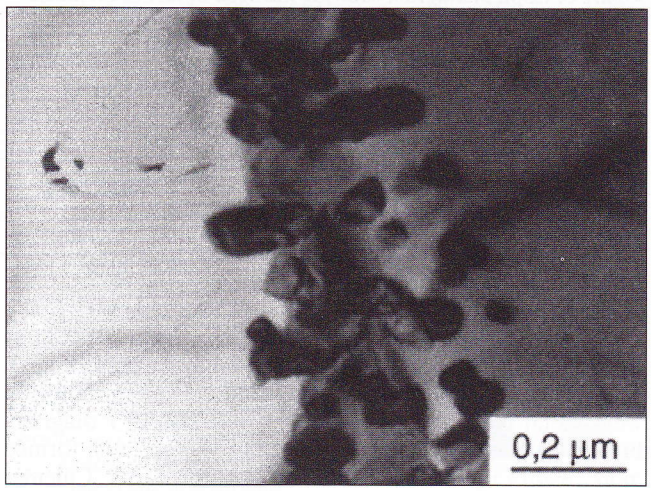

Figure 2. Intergranular Cr_2N formed in 29Cr8Ni2Mo weld metal in as-welded condition.

Figura 2. Nitruri intergranulari del tipo Cr_2N precipitati nel materiale 29Cr8Ni2Mo non trattato.

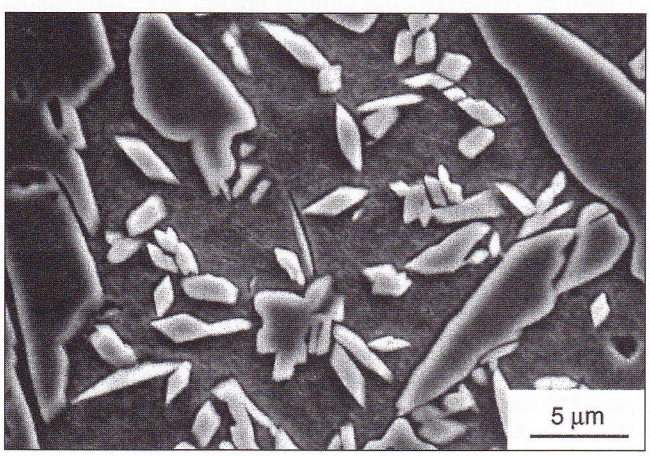

Figure 3. SEM micrograph showing secondary austenite in 29Cr8Ni2Mo weld metal.

Figura 3. Micrografia SEM con evidenziata l'austenite secondaria formatasi nel cordone 29Cr8Ni2Mo.

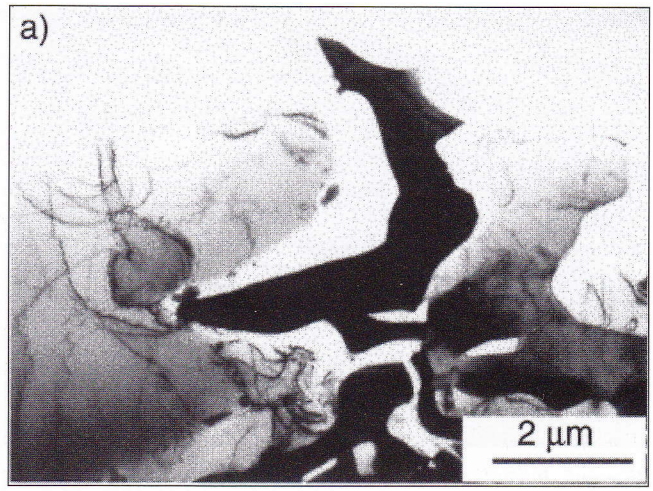

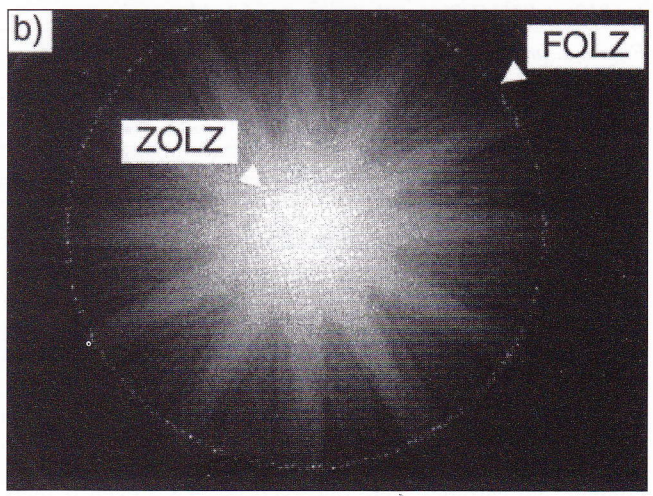

Figure 4. a) TEM micrograph illustrating sigma phase formed in 29Cr8Ni2Mo weld metal heat treated at 850°C for 810 s. b) Corresponding CBED pattern.

Figura4. (a) Immagine TEM della fase sigma precipitata nel cordone 29Cr8Ni2Mo trattato a 850°C per 810s, e (b) corrispondente immagine di diffrazione a fascio convergente (CBED).

cles were observed and much smaller particles with eutectoid structures were present at lower temperature. Sigma phase first formed at δ/δ/γ triple points and later at ferrite/austenite phase boundaries and often resulted in a typical eutectoid structure of σ and γ_2 in prior ferrite grains. SAED and CBED patterns were used to identify σ (Figure 4). Sigma phase and matrix had no fixed orientation relationship but in some cases it exhibited the crystallographic relation ⟨001⟩σ//⟨111⟩δ with the ferritic matrix. Careful analyses in ATEM and SEM showed no evidence of χ-phase in 29.8.2 weld metal whereas this phase was observed in 25.10.4 for short heat treatment times. In weld metal type 25.10.4 χ phase tended to precipitate in the narrow ferrite arms while σ phase precipitated essentially in the broad ferrite arms. Conventional diffraction patterns showed the orientation relationship ⟨011⟩χ//⟨011⟩δ, which is consistent with the expected cube to cube orientation. As a consequence the nucleation of χ phase at ferrite grain boundaries is facilitated and this phase may act as a nucleation site for sigma phase. Isothermal heat treatment resulted in the precipitation of intergranular Cr_2N mainly located at δ/γ phase boundaries but it should be pointed out that also intragranular Cr_2N were observed. Simultaneous precipitation of secondary austenite occurred during heat treatment as demonstrated in Figure 5 obtained using backscattered electrons in SEM.

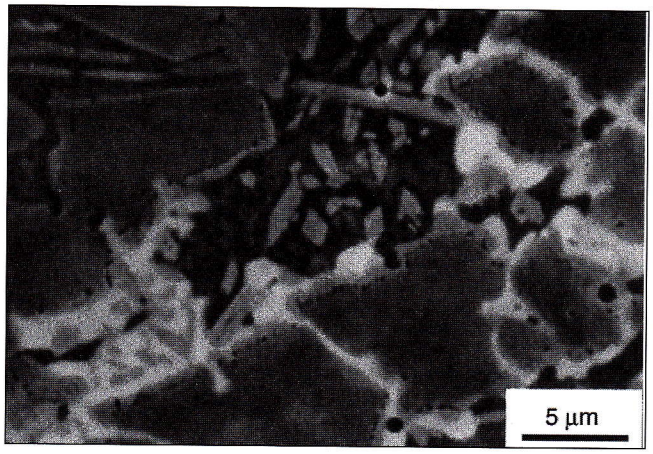

Figure 5. Backscattered electron image showing the simultaneous formation of γ_2 (light grey) and Cr_2N (black) in 29Cr8Ni2Mo aged for 810s at 850°C. Sigma phase appears in white contrast.

Figura 5. Immagine SEM, ottenuta con gli elettroni retrodiffusi, che evidenzia la precipitazione di fase σ (bianca) e di γ_2 (grigia) in cooperazione con Cr_2N (neri), dopo trattamento a 850°C per 810s.

THERMODYNAMIC CALCULATION

The computer program Thermo-Calc [15] was used to predict the stability of occurring phases as a function of temperature and composition in 29Cr8Ni2Mo weld metal. Figure 6 represents an isopleth diagram showing the phases predicted under equilibrium conditions for 29.8.2 weld metal and their stability as a function of temperature and nitrogen concentration.

Carbides are less important in super duplex stainless steels than in traditional stainless steels because of the low carbon content. No carbides were observed in 29.8.2 even if thermodynamic calculation predicted a very low fraction of $M_{23}C_6$. Large amounts of chromium and molybdenum in DSS increase both the kinetics and the volume fraction of sigma phase and expand its stability interval. One important conclusion to be drawn from the thermodynamic calculation is that nitrogen addition decreases the upper temperature limit of stability of $M_{23}C_6$ and sigma phase, even if this effect is small for σ-phase. Moreover, in the case of Cr_2N (ε), nitrogen is predicted to increase the stability limit markedly.

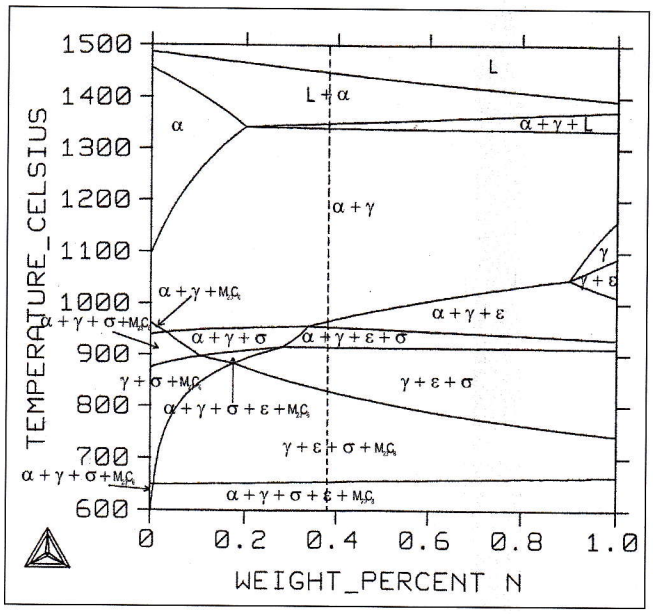

Figure 6. Isopleth diagram showing nitrogen influence on phase stabilities in 29Cr8Ni2Mo.

Figura 6. Diagramma di stato calcolato con Thermo-Calc che mostra l'effetto dell'azoto sulla stabilità delle fasi presenti nel cordone 29%Cr-8%Ni-2%Mo.

TTT AND CCT DIAGRAMS

The nose of the C-curve relative to intermetallic phase precipitation is located at 850°C for the 29Cr8Ni2Mo weld metal whereas for the 25Cr10Ni4Mo it is located at 900°C and the stability interval of intermetallic phase is restricted as shown by the lower dissolution temperature found in 29.8.2. The faster kinetics of intermetallic phase precipitation in weld metal type 25.10.4 is evident from the TTT diagram. Figure 7 illustrates that 1 pct intermetallic phase is formed more readily in 25.10.4 weld metal than in 29.8.2. Calculated CCT diagrams are shown in Figure 8. The upper part and the lower part of the CCT curves correspond to the time necessary to form 1 pct and 2 pct respectively of intermetallic phase during cooling. The cooling rates corresponding to curves A through F are 8, 16, 32, 64, 128, 256 °C/min re-

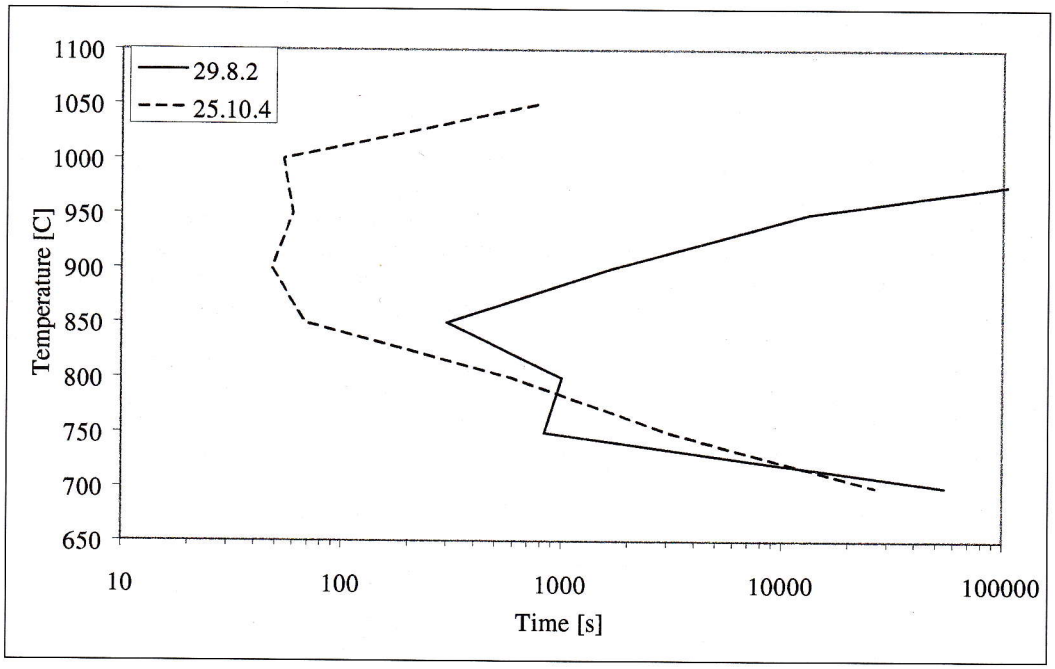

Figure 7. TTT diagram showing C curves representing 1% of intermetallic phase.

Figura 7. Diagramma TTT relativo alla formazione dell'1% di fase σ in cordoni di saldatura di tipo 29%Cr-8%Ni-2%Mo-0.4%N e 25%Cr-10%Ni-4%Mo-0.28%N.

Figure 8. Calculated CCT curves corresponding to 1% and 2% respectively of intermetallic phase formed during cooling.

Figura 8. Diagramma CCT relativo alla formazione dell'1% e del 2% di fase intermetallica.

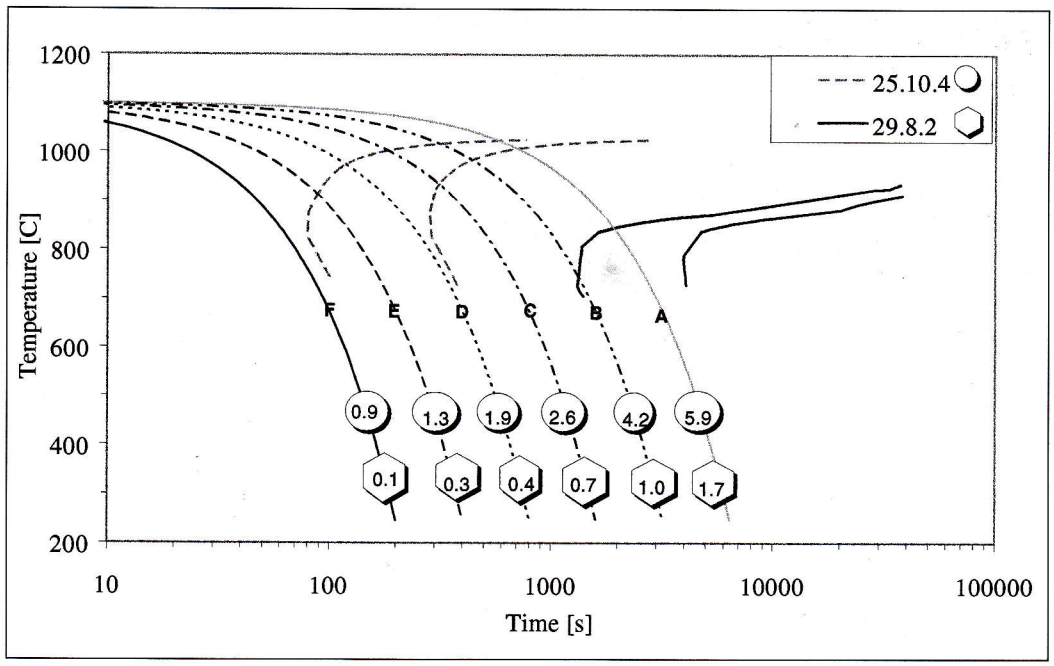

Figure 9. Concentration of alloying element in Widmanstätten and vermicular ferrite of 25Cr10Ni4Mo (SD) and 29Cr8Ni2Mo (SDN) (as welded condition) obtained using EDX in SEM, the error bars representing the standard deviation of 10 separate measurements.

Figura 9. Composizione chimica (% in peso), di δ e γ nelle zone Widmanstätten e Vermicolari, ottenuta tramite analisi EDX al SEM del materiale non trattato.

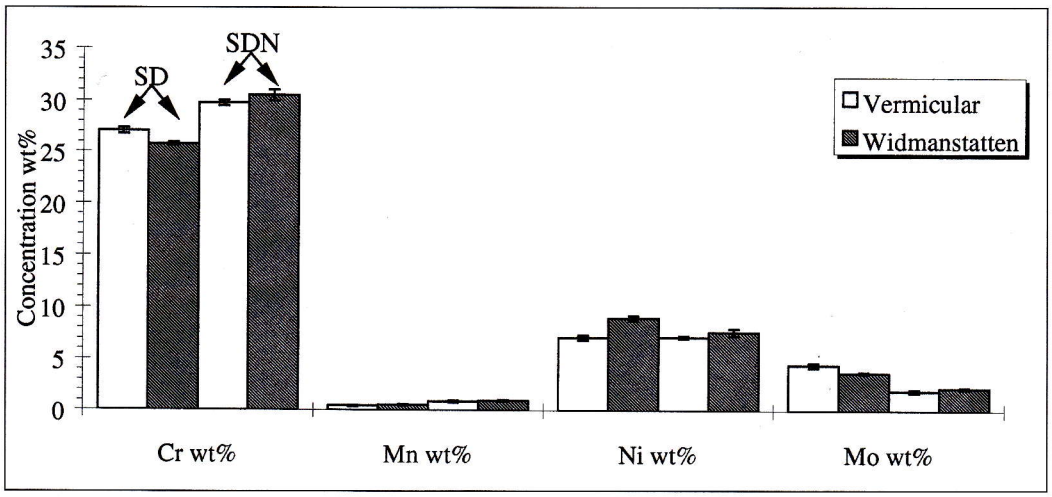

spectively, while the number in circles and hexagons represent the percentage of intermetallic phase resulting at room temperature. The critical cooling rates necessary to form 1, 2 and 5 pct of intermetallic phase are much slower for 29.8.2 weld metal than for 25.10.4.

CHEMICAL ANALYSIS

The concentration of alloying elements in austenite, ferrite and sigma phase measured using EDX in SEM showed that in 25.10.4 weld metal the vermicular ferrite was richer in chromium and molybdenum and poorer in nickel compared with ferrite in Widmanstätten areas. On the contrary, no significant differences were observed in 29.8.2 weld metal between normal duplex and vermicular microstructures as shown in Figure 9. Secondary austenite was leaner in Cr and Mo and richer in Ni compared with primary austenite particularly in weld metal type 25.10.4. Since the weld metal is a highly metastable structure, partitioning of alloying elements occurs during heat treatment resulting in a redistribution of δ-forming elements in ferrite and γ-forming elements in austenite. Sigma phase was enriched with respect to chromium, molybdenum and silicon but lean with respect to nickel and iron compared to the ferritic-austenitic matrix. The concentrations of Si, Cr, Mo increased whereas Ni and Fe concentrations decreased with the ageing time. The EDX analysis showed that σ phase in 29.8.2 aged for 72 h at 850°C is enriched in Cr and lower in Mo compared to the weld metal type 25.10.4.

DISCUSSION

Welding of 29Cr8Ni2Mo and 25Cr10Ni4Mo with nitrogen addition in the shielding gas resulted in a weld metal composed of "normal" duplex regions, characterised by primary ferrite grains with Widmanstätten type austenite and "vermicular" areas where δ had a lath-like or vermicular morphology forming an almost continuous network. The vermicular regions solidified in a ferritic-austenitic mode rather than an entirely ferritic mode. In the as welded conditions no intermetallic phase was observed in the weld metals but minor precipitation of intergranular Cr_2N mainly located at δ/γ phase boundaries took place during rapid cooling of the nitrogen rich 29.8.2 weld metal. The higher nitrogen concentration of 29.8.2 weld metal is expected to enhance the kinetics of primary austenite formation, thereby reducing the driving force for precipitation of γ_2 during for instance reheating [4]. EDX analysis showed that in all weld metals γ_2 has a significantly lower concentration of both Cr and Mo and a higher concentration of Ni compared with the primary austenite.

Quantitative image analysis has clearly shown a higher stability of 29.8.2 weld metal compared with 25.10.4 with respect to intermetallic phase formation and this effect is most pronounced at high temperature. In addition, the lower molybdenum content of 29.8.2 diminishes the temperature interval of stability of intermetallic phases. As clearly illustrated in Figure 10 calculations using the computer program Thermo-Calc showed that the driving force for σ-phase decreased with additions of nitrogen. This is explicable in physical terms as a lower activity of chromium and molybdenum in the presence of nitrogen.

It is clear from the TTT and CCT diagrams that the precipitation kinetics of intermetallic phase is significantly faster in molybdenum-rich weld metals (type 25.10.4) than in 29.8.2. Careful analysis in ATEM and SEM showed that 29.8.2 weld metal was virtually devoid of χ-phase, presumably because of the low molybdenum content, whereas this phase was observed in weld metal of type 25.10.4 particularly at the early stages of precipitation.

Tilting experiments performed in ATEM have shown that ferrite and austenite in the vermicular zone do not obey the Kurdjumov-Sachs orientation relationship thereby resulting in high energy δ/γ phase boundaries. Furthermore, an enrichment of molybdenum and chromium in ferrite of vermicular appearance was observed by EDX analysis in SEM. This effect is most likely related to the ferritic-austenitic solidification mode [16]. The deviation from Kurdjumov-Sachs orientation relationship and the enrichment of molybdenum and chromium in combination offer a rationale of the preferential precipitation of intermetallic phase in vermicular areas.

Observation in ATEM showed that χ phase precipitated more readily in narrow ferrite arms of 25.10.4 weld metal particularly in the vermicular area thereby acting as a precursor to σ-phase by providing suitable nucleation sites. This mechanism, identified in previous work on DSS weld metal [17], was directly verified also in the present work.

CONCLUSIONS

The higher nitrogen content of 29Cr8Ni2Mo suppresses the formation of γ_2 precipitates. This effect is explicable in terms of enhanced kinetics of primary austenite formation whereby the driving force for secondary austenite formation is reduced correspondingly. The intragranular secondary austenite precipitated in the Widmanstätten reheated zone was found to be leaner than the primary austenite with respect to molybdenum and chromium.

The new 29Cr8Ni2Mo weld metal showed a high stability with respect to σ-phase and χ-phase formation. Thermodynamic calculations showed a lower driving force for intermetallic phase precipitation linked to a lower activity of chromium and molybdenum in the presence of high nitrogen concentrations.

It can be concluded from this investigation that the lower molybdenum concentration in association with the beneficial effects of nitrogen in reducing the activities of molybdenum and chromium offer a likely explanation for the microstructural stability of type 29Cr8Ni2Mo weld metal. The situation is further improved by the absence of χ-phase, which may act as precipitation nuclei in more highly alloyed filler metals.

ACKNOWLEDGEMENTS

This paper is published with the permission of AB Sandvik Steel. Supporting colleagues at AB Sandvik Steel are gratefully acknowledged. The support of Mr P. Kangas and the assistance of Mr M. Lundström in performing the Thermo-Calc calculations are particularly acknowledged.

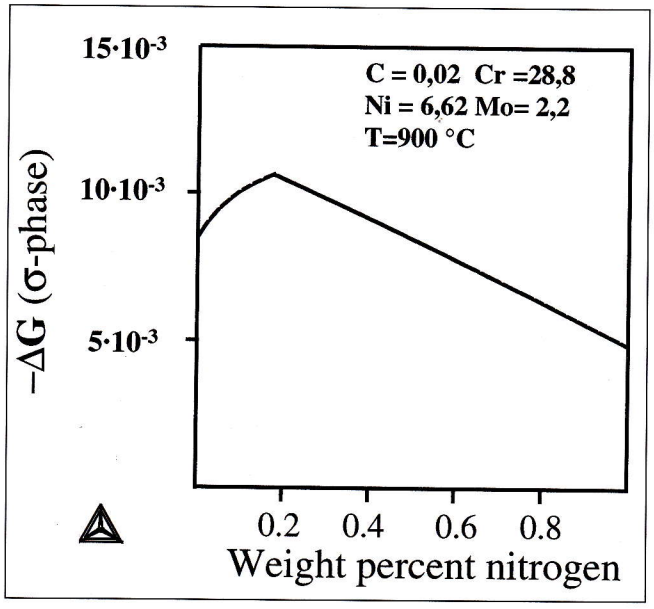

Figure 10. Thermo-Calc calculation showing the effect of nitrogen on the driving force for σ-phase.

Figura 10. Analisi effettuata con Thermo-Calc in cui è illustrato l'effetto dell'azoto sulla forza motrice della reazione di formazione della fase sigma.

REFERENCES

1) J. CHARLES, Proc. Duplex stainless Steels '91, Beaune (1991), Les Éditions de Physique, Paris (1991), p. 3
2) J.-O. NILSSON, Mater. Sci. Technol. 8, (1992), p. 685.
3) M. LILJAS and J.-O. NILSSON, Mater. Sci. Forum 318-320, (1999), p. 189.
4) S. HERTZMAN, T. HUHTALA, L. KARLSSON, J.-O. NILSSON, M. NILSSON, R. JARGELIUS-PETTERSSON and A. WILSON, Mater. Sci. Technol. 13, (1997), p. 604.
5) J.-O. NILSSON, L. KARLSSON and J.-O. ANDERSSON, Mater. Sci. Technol. 11, (1995), p. 276.
6) B. BONNEFOIS, F. DUPOIRON and J. CHARLES, Proc. Duplex stainless Steels '94, Cambridge (1994), TWI, Cambridge (1994), Paper 87.
7) T. GOOCH, Proc. Duplex stainless Steels '91, Beaune (1991), Les Éditions de Physique, Paris (1991), p. 325.
8) M. AVRAMI, J. Chem. Phys. 7, (1939), p. 1103.
9) M. AVRAMI, J. Chem. Phys. 8, (1940), p. 212.
10) M. AVRAMI, J. Chem. Phys. 9, (1941), p. 177.
11) E. SCHEIL, Arch. Eisenhüttenwesen 8, (1935), p. 565.
12) A. WILSON J.-O. NILSSON, Scand. J. Metall. 25 (1996), p. 178.
13) A. GREGORI, J.-O. NILSSON and F. BONOLLO, Mater. Sci. Forum 318-320, (1999), p. 829.
14) N. SUUTALA, Acta Univ. Oulu C26, Oulu (1983), p. 53.
15) B. SUNDMAN, B. JANSSON and J.-O. ANDERSSON, Calphad 9, (1985), p. 153.
16) L. KARLSSON, S. PAK and S.L. ANDERSSON, Proc. Conf. Stainless Steel '91, ISIJ, Chiba (1991), p.1093.
17) J.-O NILSSON, T. HUHTALA, P. JONSSON, L KARLSSON and A. WILSON, Metall. Mater. Trans. 27A, (1996), p. 2196.

ABSTRACT

ANALISI QUANTITATIVA E MODELLIZZAZIONE TERMODINAMICA DELLA STABILITÀ MICROSTRUTTURALE DI UN NUOVO MATERIALE D'APPORTO SUPER DUPLEX ALTOLEGATO IN AZOTO

La richiesta di materiali dalle prestazioni sempre più elevate in termini di resistenza alla corrosione e di proprietà meccaniche in condizioni particolarmente critiche, è stata il motore dello sviluppo di nuovi acciai inossidabili super duplex. Questi acciai, avendo tenori sempre più elevati di elementi in lega, presentano caratteristiche superiori rispetto agli acciai duplex grazie alla loro elevata resistenza alla corrosione localizzata. Per contro, elementi quali il cromo ed il molibdeno, pur aumentando la resistenza al pitting, accrescono anche il rischio di precipitazione di fasi intermetalliche quali la fase sigma. La recente introduzione di nuovi acciai inossidabili superduplex altolegati in azoto appare estremamente promettente, costituendo una valida soluzione ai problemi di stabilità microstrutturale dei super duplex tradizionali.

Lo sviluppo di materiali d'apporto dedicati è prerequisito essenziale per garantire giunti saldati di qualità, con proprietà meccaniche e di resistenza alla corrosione paragonabili a quelle del metallo base. In questo studio vengono evidenziate le caratteristiche microstrutturali di un cordone di saldatura del tipo 29%Cr-8%Ni-2%Mo-0.4%N ottenuto con il procedimento GTAW, impiegando un nuovo materiale d'apporto appositamente sviluppato per la saldatura dei nuovi super duplex altolegati in azoto.

I risultati sperimentali hanno evidenziato che l'introduzione in lega di tenori elevati di azoto ha permesso di ridurre sensibilmente la formazione di austenite secondaria, nota per i suoi effetti negativi sulla resistenza al pitting. L'incremento del tenore di azoto, favorendo la formazione di austenite primaria ed aumentando la stabilità della struttura ferritico-austenitica, riduce, infatti, il rischio di precipitazione di questa fase nel corso di passate successive. Inoltre, il nuovo metallo d'apporto ha una microstruttura ben bilanciata e più stabile, rispetto ai normali superduplex con il 4% di molibdeno, nei confronti della precipitazione di fasi intermetalliche. Contrariamente a quanto osservato nei super duplex tradizionali, l'analisi eseguita al TEM ha evidenziato che la fase sigma è l'unica fase intermetallica presente nell'intervallo 700-1100°C. La fase χ, nota per fornire siti preferenziali di nucleazione della fase sigma, è del tutto assente. Quanto osservato è riconducibile sia al ridotto tenore di molibdeno, sia all'elevata concentrazione d'azoto del materiale d'apporto, che favorisce la stabilizzazione della microstruttura. L'analisi termodinamica ha, infatti, evidenziato che l'azoto ha un duplice effetto sulla precipitazione di fasi intermetalliche. L'aumento del tenore in lega di questo elemento restringe il campo di stabilità dei carburi e della fase sigma, e, diminuendo l'attività di elementi sigma-formatori quali il cromo ed il molibdeno, ritarda la decomposizione della ferrite.

Si può quindi concludere che il minor tenore di molibdeno, associato agli effetti benefici dell'azoto nel diminuire l'attività del cromo e all'assenza di fase c, costituisce una valida spiegazione della elevata stabilità microstrutturale del nuovo metallo d'apporto del tipo 29%Cr-8%Ni-2%Mo-0.4%N.